数理解析研究所講究録
第 696 巻 1989 年 204-221

Homoclinic Linkage in the Double Scroll Circuit and the Cusp-Constrained Circuit

R.Tokunaga, T.Matsumoto, T.Ida, and K.Miya

Department of Electrical Engineering, Waseda University, Tokyo 160, Japan.

I. Introduction

This paper reports ***Homoclinic Linkage***. In this paper, we will deal with two circuits. One is the Double Scroll circuit [1] whose dynamics is given by

$$\begin{aligned}\frac{dx}{d\tau} &= \alpha\{y - \frac{2}{7}x + \frac{3}{14}(|x+1| - |x-1|)\}\\ \frac{dy}{d\tau} &= x - y + z\\ \frac{dz}{d\tau} &= -\beta y\end{aligned} \qquad (1)$$

which is symmetric with respect to the origin. The other is the Cusp-Constrained circuit [2] whose dynamics is given by

$$\begin{aligned}\frac{dx}{d\tau} &= -y + ax\\ \varepsilon\frac{dy}{d\tau} &= \frac{3}{4}\{|y + z| - |y - z|\} + \frac{1}{2}y + x\\ \frac{dz}{d\tau} &= \frac{3}{4}\{|y + z| - |y - z|\} + (\frac{1}{2}-c)z - 1\end{aligned} \qquad (2)$$

which is symmetric with respect to the z-axis. The parameters α, β, a, c and ε are functions of circuit parameters. In order to show what homoclinic linkage is, we will focus our attention on (1).

/

1.1 Fates of Periodic Orbits

Let us fix $\beta = 9.0$, and see what happens to (1) as we vary α. The dynamics has three equilibria: **O**, the origin, $\mathbf{P}^+$ and $\mathbf{P}^-$ (Fig.1). The last two are located symmetrically with respect to **O**, because of the symmetry of (1). For α small, $\mathbf{P}^\pm$ are *sinks*. For $\alpha=\alpha_0 \cong 5.118$, Hopf bifurcation at $\mathbf{P}^\pm$ gives rise to a pair of nonsymmetric *stable* periodic orbits ($\Pi^1{}_0$) and a symmetric *saddle type* periodic orbit (Π^1) (Fig.1). At $\alpha=\alpha_{p1}$, $\Pi^1{}_0$ loses its stability to give rise to a new periodic orbit $\Pi^2{}_0$ via period doubling bifurcation. However $\Pi^1{}_0$ still survives as a saddle type periodic orbit. Our first question is

What is the fate of these two periodic orbits, $\Pi^1{}_0$ and Π^1 ?

Figure 2 shows how these periodic orbits are deformed as we very α where the ordinate is *period*† of the periodic orbits. A broken (resp. solid) curve indicates that the periodic orbit is unstable (resp.stable). α_{t1}, α_{t2}, α'_{t1}, α'_{t2}, (resp. α_{p1}, α_{p2}, α'_{p1}, α'_{p2}) indicate the values of α at which *saddle-node* (resp. period doubling or pitch folk) bifurcations take place. Both of the curves *oscillate* around $\alpha \cong 7.2978$ at which the simplest homoclinicity ($\Gamma^1{}_0$) through **O** exists.(Fig.4(a)) And the period tends to $+\infty$. It seems that $\Pi^1{}_0$ and Π^1 are deformed into $\Gamma^1{}_0$. We can confirm that this continuous deformation via observing trajectories. (Fig.3) Hence the answer to the above question is

$\Pi^1{}_0$ and Π^1 are continuously deformed into *homoclinic orbit* $\Gamma^1{}_0$.

This has been observed by George[3].

Next we observe the fate of other periodic orbits $\Pi^2{}_0$ and $\tilde{\Pi}^2{}_0$ (resp. $\Pi^1{}_1$ and $\tilde{\Pi}^1{}_1$) which are born via period doubling of $\Pi^1{}_0$ at $\alpha = \alpha_{p1}$ and $\alpha = \alpha_{p2}$, (resp. pitch folk bifurcation of of Π^1 at $\alpha=\alpha'_{p1}$ and $\alpha=\alpha'_{p2}$), respectively. Figure 5 shows the bifurcation curves of these four periodic orbits.

---

† Throughout this paper, half period is used for (α, period)-bifurcation diagram of symmetric periodic orbit.

It is clearly observed that

$\Pi^2{}_0$ and $\Pi^1{}_1$ (resp. $\tilde{\Pi}^2{}_0$ and $\tilde{\Pi}^1{}_1$) are continuously deformed into homoclinic orbits $\Gamma^2{}_0$ and $\Lambda^2{}_0$ (resp. $\tilde{\Gamma}^2{}_0$ and $\tilde{\Lambda}^2{}_0$).

Recall that there are symmetric periodic orbit, Π^1 and nonsymmetric periodic orbit, $\Pi^1{}_0$ which are continuously deformed into $\Gamma^1{}_0$. The above four periodic orbits are all non-symmetric, hence the symmetry of the dynamics indicates existence of other symmetric periodic orbits which are deformed into $\Gamma^2{}_0$, $\Lambda^2{}_0$, $\tilde{\Gamma}^2{}_0$ and $\tilde{\Lambda}^2{}_0$. Figure 5 shows the bifurcation curves of a pair of symmetric orbits, Π^2 and $\tilde{\Pi}^2$, which are shown in Fig.6.

An extremely interesting fact is that

different homoclinicities, $\Gamma^2{}_0$ and $\Lambda^2{}_0$ (resp. $\tilde{\Gamma}^2{}_0$ and $\tilde{\Lambda}^2{}_0$) are linked together via Π^2 (resp. $\tilde{\Pi}^2$).

From the above observation, the fate of periodic orbits are classified by the following:

(T1) periodic orbits whose bifurcation curve is terminated by a ***Hopf bifurcation*** and ***homoclinicity***;
(T2) periodic orbits whose bifurcation curve is terminated by a ***period doubling*** (resp. ***pitch folk bifurcation***) and ***homoclinicity***;
(T3) periodic orbits whose bifurcation curve is terminated by ***two homoclinicities*** .

Especially, (iii) is very important because these curves are isolated from other curves. We call this case a

homoclinic linkage.

Next, let us observe the above bifurcation from a different view point. Figure 7 shows $(\Gamma^2_0, \Lambda^2_0)$ and $(\tilde{\Gamma}^2_0, \tilde{\Lambda}^2_0)$ in the (α, y^*, z^*)-space instead of the (α, T)-space, where y^* and z^* are defined by the following: Let

$$U = \{(x,y,z) | \; x = 1\}. \tag{3}$$

Then $(1, y^*, z^*)$ is the point at which a periodic orbit hits U. Note that locus of each periodic orbit in this space is an infinite spiral as it approaches homoclinicity.

1.2 The Shilnikov Condition

The mechanism of continuous deformation of a periodic orbit into a homoclinicity is studied in [4][5]. Roughly speaking, the mechanism can be classified by the following: Suppose that a homoclinicity in question has one real eigenvalue $\gamma > 0$ and a complex-conjugate pair $\sigma \pm j\omega$, $\sigma < 0$.

(i) If

$$\gamma > |\sigma| \tag{4}$$

then the bifurcation curve associated periodic orbit oscillates infinite times around homoclinicity, (see Fig.8(a)), while

(ii) if

$$\gamma < |\sigma|, \tag{5}$$

then the bifurcation curve associated with periodic orbit oscillates only finite times around homoclinicity. (see Fig.8(a))

Since condition (4) is one of the conditions of the theorem of Shilnikov [6], we call this condition the *"Shilnikov condition"*. Naturally, then, the end of a spiral is characterized by

$$\gamma = |\sigma|. \tag{6}$$

II. Homoclinic Linkages in the Double Scroll Circuit

In the previous section, we observed (Γ^2_0,Λ^2_0) and $(\tilde{\Gamma}^2_0,\tilde{\Lambda}^2_0)$ at β=9.0. However these homoclinic linkages are deformed into $(\Gamma^2_0,\tilde{\Gamma}^2_0)$ and $(\Lambda^2_0,\tilde{\Lambda}^2_0)$, as β decreases. (see Fig.9(a)) Moreover homoclinic linkages disappear at β=1.95. (Fig.9(b)) In order to analyze this mechanism, we construct a sheet model in the (α^*,β,s)-space, where α^* and s are defined by

$$\alpha^* \stackrel{\Delta}{=} \alpha - H(\beta),$$
$$s \stackrel{\Delta}{=} y^* + 3z^*,$$

respectively. Here, $H(\beta)$ denotes the value of α for which homoclinicity Γ^1_0 occurs. The coordinate "s" contains the information as to where a periodic orbit is located. The purpose of taking the linear combination of y* and z* instead of y* or z* alone is simply to avoid self-intersection of the loci. Figure 10 shows a hand drawn sheet model. The computer generated model is shown in Fig.11. In this space, periodic orbit corresponds to a continuous sheet. The sheet model of Fig.10 consists of the following three sheets:

(1) S_0^2 which is terminated by homoclinicity locus $\Gamma^2_0 \cup \tilde{\Gamma}^2_0$ and period doubling bifurcation set $P_l \cup \tilde{P}_l$;

(2) S_1^1 which is terminated by homoclinicity locus $\Lambda^2_0 \cup \tilde{\Lambda}^2_0$ and pichfolk bifurcation set $P_r \cup \tilde{P}_r$;

(3) S^2 which is terminated by homoclinicity loci $\Gamma^2_0 \cup \tilde{\Gamma}^2_0$ and $\Lambda^2_0 \cup \tilde{\Lambda}^2_0$.

Note that Γ^2_0 and $\tilde{\Gamma}^2_0$ (resp. Λ^2_0 and $\tilde{\Lambda}^2_0$) and other bifurcation sets connect to each other in the (α,β)-space. Note that homoclinic linkage in the (α,β)-space is S^2, itself. Hence, it is sufficient to analyze S^2 in order to analyse homocliniclinkage via Π^2.

The sections in Figure 10 are planes which are normal to the β-axis. Consider the intersection between S^2 and section-0 which consists of continuous curves corresponding to $(\Gamma^2_0, \Lambda^2_0)$ via Π^2 and $(\tilde{\Gamma}^2_0, \tilde{\Lambda}^2_0)$ via $\tilde{\Pi}^2$. A pair of saddle node bifurcation sets, T_l and T'_l, are born out of cusp-point C_l. On the other hand, $\tilde{\Pi}^2$ contains another saddle node bifurcation sets, $\tilde{T}_l$ and $\tilde{T}_r$. T_l hits $\tilde{T}_l$ at S_l on section-1. Here on section-1, a pair of linkages merge togethor and form the $(\Gamma^2_0,\Lambda^2_0,\tilde{\Gamma}^2_0,\tilde{\Lambda}^2_0)$-linkage. Below section-1, the linkage is devided into $(\Gamma^2_0, \tilde{\Gamma}^2_0)$ and $(\Lambda^2_0, \tilde{\Lambda}^2_0)$. Between section-1 and section-2, a pair of saddle node bifurcation sets, T_r and T'_r are born out of another cusp-point C_r. On section-2, $(\Lambda^2_0,\tilde{\Lambda}^2_0)$ touches itself at S_r. Hence, under section-2, this homoclinic linkage breaks into two parts: one is loop-like set containing T'_l and T'_r, while the other is $(\Lambda^2_0, \tilde{\Lambda}^2_0)$.

2.2 Disappearance of Homoclinic Linkages

As β decreases further, Γ^2_0 and $\tilde{\Gamma}^2_0$ (resp.Λ^2_0 and $\tilde{\Lambda}^2_0$) get closer to each other. Finally they merge, and then homoclinic linkages disappear. In the same manner, period doubling (resp. pitch folk) bifurcation sets P_l and $\tilde{P}_l$ (resp. P_r and $\tilde{P}_r$) disapear. Hence for β small, only Π^1_0 and Π^1 which are connected via Γ^1_0 survive.

III. Homoclinic Linkages in the Cusp-Constrained Circuit

In this section, we consider (2) with $\varepsilon \to 0$.

3.1 Geometric Structure and Homoclinicities

Figure 12 shows the constrained surface Σ which is given by

$$3/4\ \{|y+z| + |y-z|\} + 1/2y + x = 0. \qquad (8)$$

Let us consider the (y,z)-projection and define subsets by

$$\mathbf{F}_{\pm} = \{(y,z) \mid z = \pm y \geq 0\}$$
$$\mathbf{F}^{c}_{\pm} = \{(y,z) \mid z = \pm\frac{1}{5}y \geq 0\}$$
$$\mathbf{L}_{+} = \{(y,z) \mid z = -y \leq 0\}$$
$$\mathbf{L}_{-} = \{(y,z) \mid z = y \leq 0\}$$
$$\mathbf{p}_{\pm} = \left(\frac{\pm 3a}{(4-c)a+2c+1}, \frac{a-2}{(4-c)a+2c+1}\right)$$
$$\mathbf{p}_{o} = \left(0, -\frac{1}{c+2}\right)$$
$$\mathbf{o} = (0,0)\ .$$

$\mathbf{F}_{\pm}$, $\mathbf{F}^{c}_{\pm}$ and $\mathbf{o}$ indicate "fold", "shadow of fold" and "cusp-point" on Σ, respectively, while $\mathbf{p}_{\pm}$ and $\mathbf{p}_{o}$ indicate fixed points of the slow vector field. If $a > 1$ and $c > -2$ hold, $\mathbf{p}_{o}$ is a saddle node. On the other hand, $\mathbf{p}_{o}$ is unstable focus in our case. Let us illustrate the behavior of the flow. (see Fig.13) Consider the intersection between righthand-side unstable manifold of $\mathbf{p}_{0}$ and $\mathbf{F}_{+}$, say $\mathbf{c}$. Let the flow which starts from $\mathbf{c}$ be denoted by $\psi^{\tau}(\mathbf{c})$. $\psi^{\tau}(\mathbf{c})$ starts to rotates around $\mathbf{p}_{+}$ in the counter clockwise direction. It hits $\mathbf{F}_{+}$ and jumps onto $\mathbf{x}_{1}$ on $\mathbf{F}^{c}_{-}$ rapidly. Next it starts to rotate around $\mathbf{p}_{-}$ in the clockwise direction, but hits $\mathbf{F}_{-}$ and jumps onto $\mathbf{x}_{2}$ on $\mathbf{F}^{c}_{+}$ rapidly. After repeating similar process which contains "jumps", it start to rotate around $\mathbf{p}_{+}$ of $\mathbf{p}_{-}$. If times of jump is even (resp.odd), it rotates around $\mathbf{p}_{+}$ (resp. $\mathbf{p}_{-}$). After several rotations, it hits $\mathbf{F}_{+}$ (resp. $\mathbf{F}_{-}$), the above "jump process" starts again.

Since (2) is a constrained system, one can not apply the definition of homoclinicity, however we would like to consider the following situations as "homoclinicity and heteroclinicity of (2)".

(i) Homoclinicity through $\mathbf{p}_{0}$ denoted by $\mathbf{H}_{0}^{n}$: unstable manifold of $\mathbf{p}_{0}$ hits cusp-point $\mathbf{o}$ after the n-th jump.

(ii) Homoclinicity and heteroclinicity through $\mathbf{p}_{\pm}$ denoted by $\mathbf{H}_{p}^{n}$:

$$\mathbf{p}_{\pm} \in \mathbf{F}^{c}_{\pm}, \text{ and} \tag{9}$$
$$\|\mathbf{x}_{n}\| > \|\mathbf{p}_{\pm}\|. \tag{10}$$

(iii) Homoclinic loop between $\mathbf{p}_\pm$ and $\mathbf{p}_o$ denoted by $\mathbf{T}^n$:
condition (9), and
$\|\mathbf{x}_n\| = \|\mathbf{p}_\pm\|$. (11)

Next let us consider the loci of homoclinicities in the (c,a)-space. An equivalent condition of (9) is given by

$a = 5.0.$ (12)

See Fig.14. $\mathbf{H}_p^n$ are located on the line segment a = 5.0, in the (c,a)-space whose right terminal point is locus of $\mathbf{T}^n$. On the other hand locus of $\mathbf{H}_o^n$ is an infinite spiral whose center is also locus of $\mathbf{T}^n$. Hence $\mathbf{H}_p^n$ and $\mathbf{H}_o^n$ are born from $\mathbf{T}^n$.

3.2 $(\mathbf{H}_p^2, \mathbf{H}_o^2)$-Homoclinic Linkages and Fish Hooks

Let us consider the $(\mathbf{H}_p^2, \mathbf{H}_o^2)$-Homoclinic Linkages. We choose c=4.9 in the (c,a)-space and find a pair of periodic orbits which are continuously deformed into $\mathbf{H}_o^2$. One of them is symmetric ($\mathbf{C}_{1/2}$) and the other is nonsymetric ($\mathbf{C}_{1/3}$). (see Fig.15) Figure 16 shows their bifurcation curves. It is clearly seen that they approach $\mathbf{H}_p^2$ at a = 5.0 with oscillatons around it. To analyse this homoclinic linkage, we construct their sheet model in the (c,a,ξ)-space where ξ is the maximal y-coordinate of the intersection between $\mathbf{F}_+$ and the periodic orbit. (see Fig.15) Figure 17 shows a hand written sheet model of the $(\mathbf{H}_p^2, \mathbf{H}_o^2)$-homoclinic linkages. It consists of a pair of sheet: one corrsponds to $\mathbf{C}_{1/2}$ ($S_{1/2}$), the other corresponds to $\mathbf{C}_{1/3}$ ($S_{1/3}$). Globally, these two sheets are scrolled with respect to $\mathbf{H}_p^2$. However its local structure near $\mathbf{T}^2$ is terminated in a very complicated manner. A pair of cusp points ($\mathbf{c}^n$) appears on $S_{1/2}$ and they are connected with each other via tangent bifurcation set (t_n). On the other hand, for c large, there is no bifurcation set on $S_{1/2}$, and $S_{1/2}$ is terminated by $\mathbf{H}_o^2$ to be connected with $S_{1/3}$. Note that this sheet model contains infinite number of cusp points $\mathbf{c}^n$ which accumulate onto $\mathbf{T}^2$. Figure 18 shows the computer generated sheet model. In the above, stability of periodic orbits is not discussed. Here we consider the region where the stable periodic orbit exists, i.e., stability interval.

In this model, period doubling bifurcation sets (p_n) (resp. pitch folk bifurcation sets (p'_n)) are located on $S_{1/3}$ ($S_{1/2}$) as in Fig.19. Dotted region in Fig.19 corresponds to stability intervals. Note that the stability interval exists along the locus of $\mathbf{H}_o^2$, and that a part of this contains single cusp point $\mathbf{c}^n$ which looks like a "fish hook". Such an accumulation structure of cusp points has been reported by Guspard et al.. [7] In their report, the nature of accumulation point has not been discussed in detail. However our case, accumulation point is defined by a codimension-2 homoclinic loop.

Acknowledgement

The authors would like to thank Dr. H.Kokubu of Kyoto University for useful coments.

References

[1] T.Matsumoto, L.O.Chua, and M.Komuro,"The Double Scroll," IEEE, Trans. CAS, Vol.CAS-32, pp.797-818, August 1985.

[2] R.Tokunaga, L.O.Chua and T.Matsumoto,"Bifurcation Analysis of A Cusp-Constrained Circuit," Int.J.C.T.A., in press.

[3] D.P.George,"Bifurcations in a piecewise linear system," Phys, Lett.A, 118, 17,1986.

[4] P.Glendinning and C.Sparrow, "Local and global behavior near homoclinic orbits," J.Stat. Phys., vol.35, pp.645-697, 1984.

[5] C.Sparrow,"The Lorenz Equation: bifurcations, chaos and strange attractors," Spring-Verlag, New York, 1982.

[6] L.P.Shilnikov, "A case of the existence of a denumerable set of periodic motions," Sov. Math. Dokl., vol.6, pp.163-166, 1965.

[7] P.Gaspard, R.Kapral and G.Nicolis, "Bifucation Phenomena near Homoclinic Syatems: A Two-Parameter Analysis," J.Stat. Phys., 35, 697, 1984.

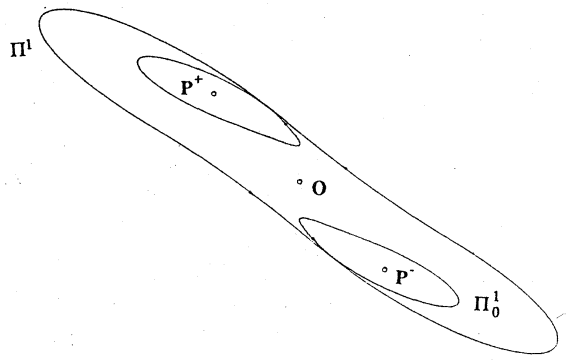

Figure 1

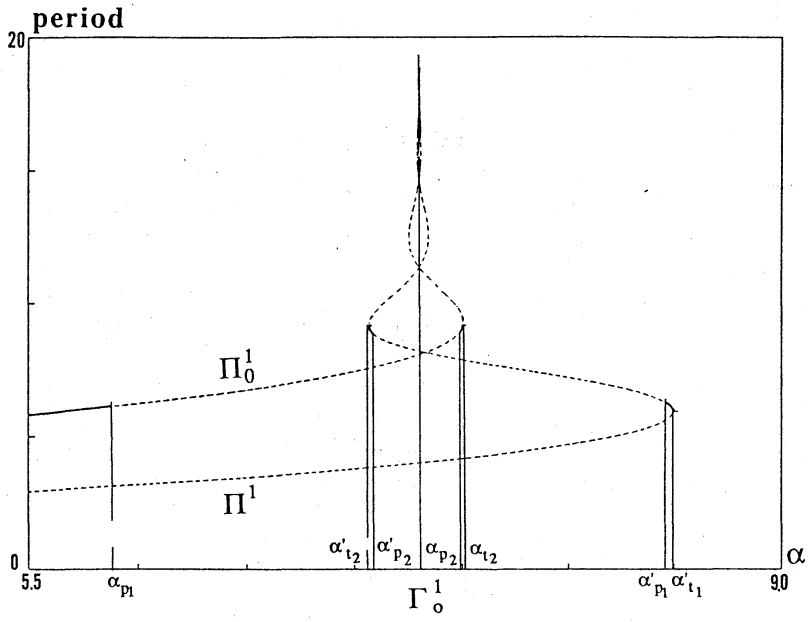

Figure 2

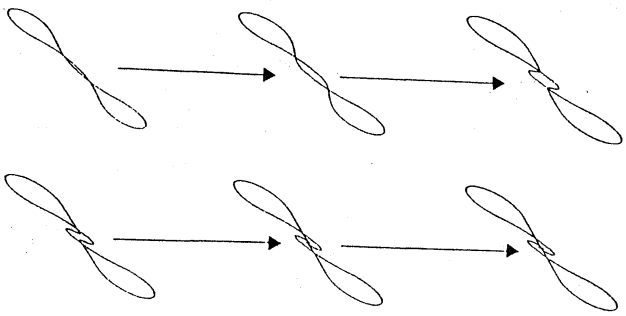

Figure 3

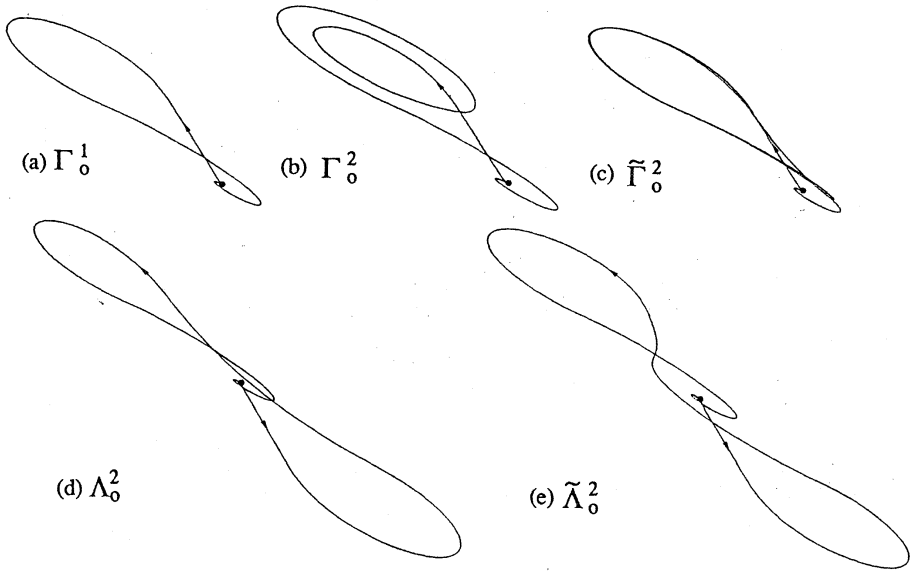

Figure 4

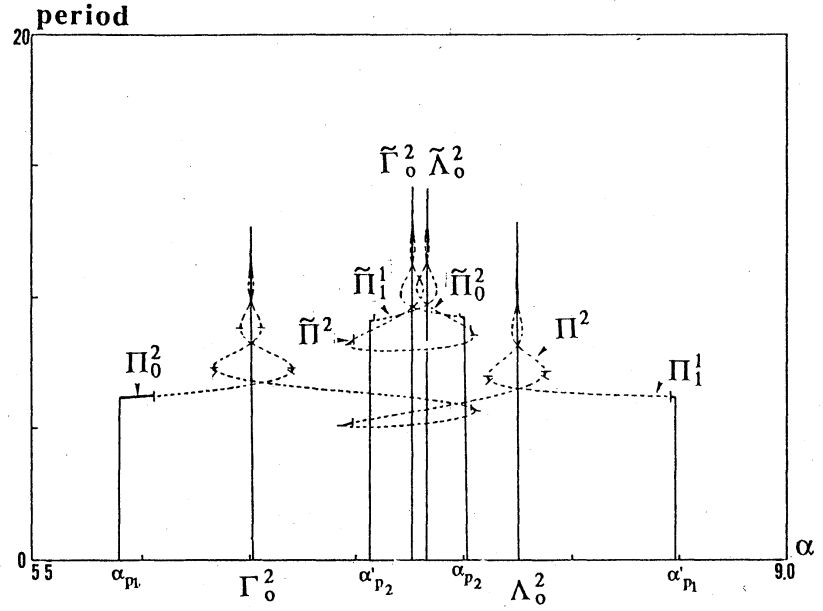

Figure 5

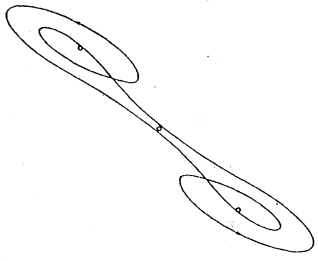

Figure 6

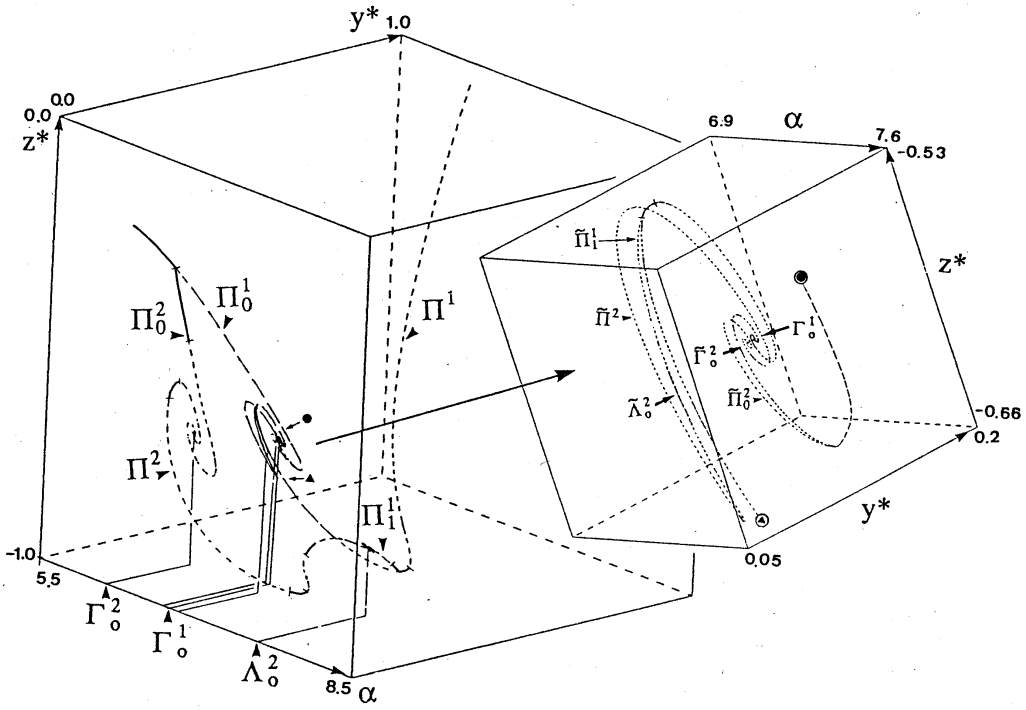

Figure 7

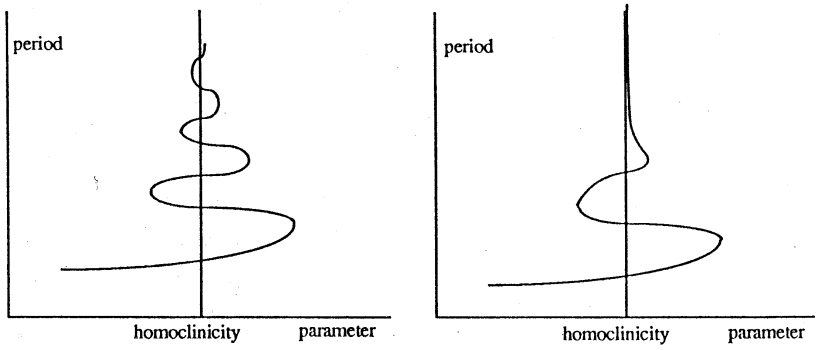

Figure 8

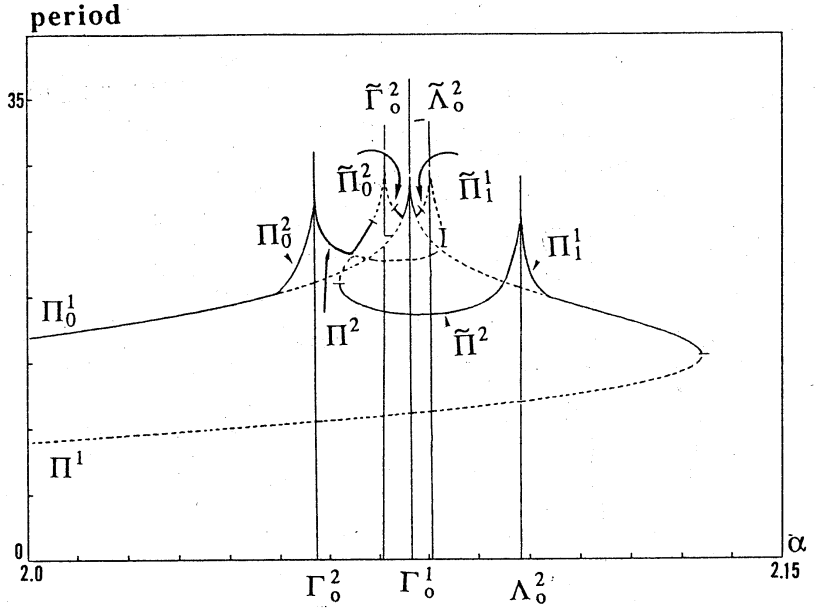
period
35
0
2.0
2.15
α
$\tilde{\Gamma}^2_o$
$\tilde{\Lambda}^2_o$
$\tilde{\Pi}^2_0$
$\tilde{\Pi}^1_1$
Π^2_0
Π^1_1
Π^1_0
Π^2
$\tilde{\Pi}^2$
Π^1
Γ^2_o
Γ^1_o
Λ^2_o

(a)

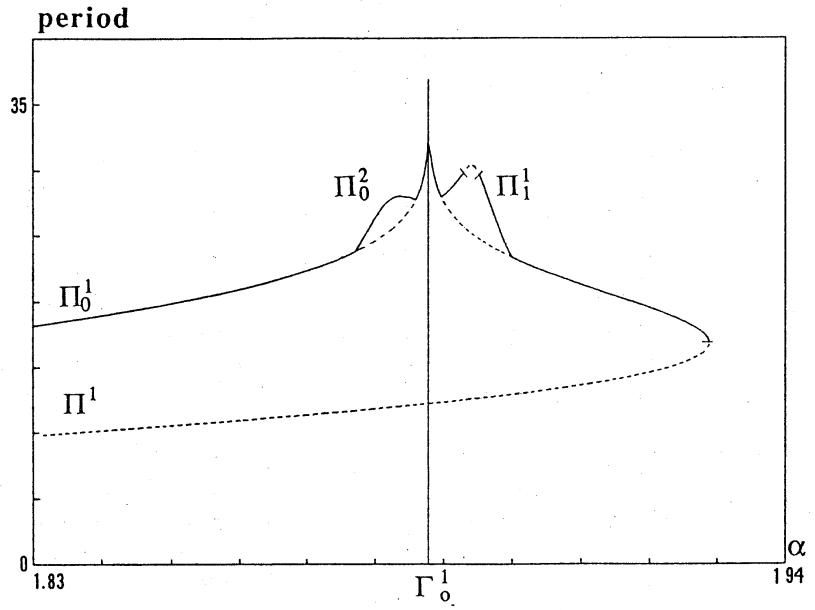
period
35
0
1.83
1.94
α
Π^2_0
Π^1_1
Π^1_0
Π^1
Γ^1_o

(b)

Figure 9

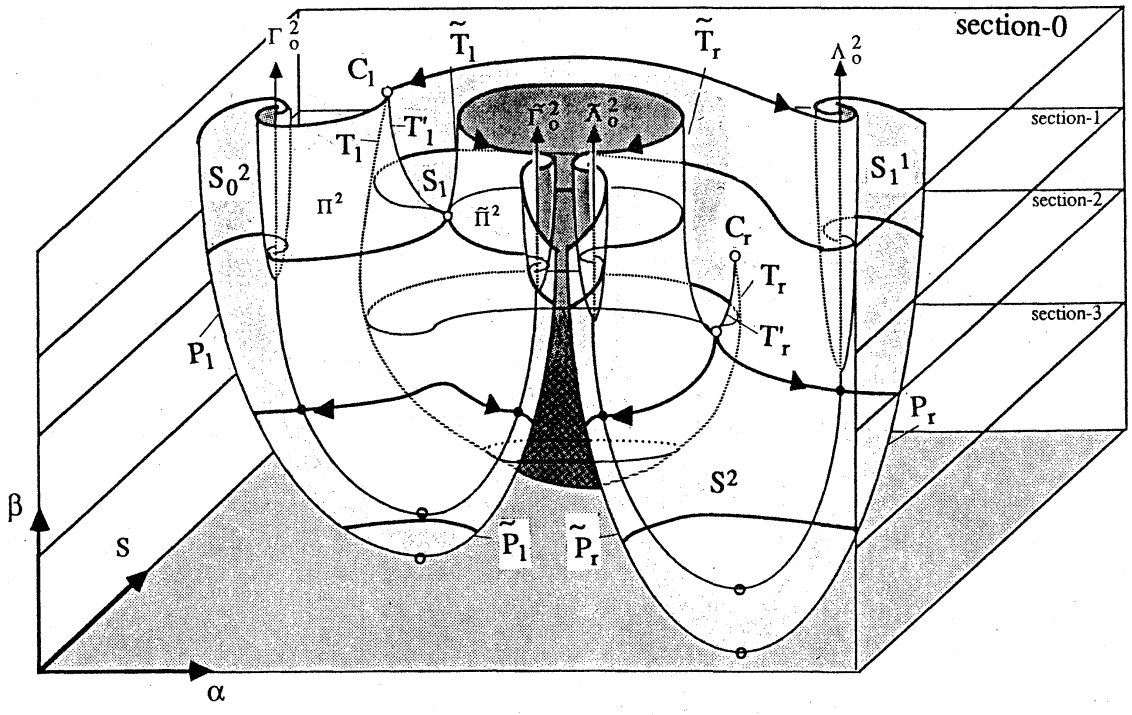

Figure 10

Figure 11

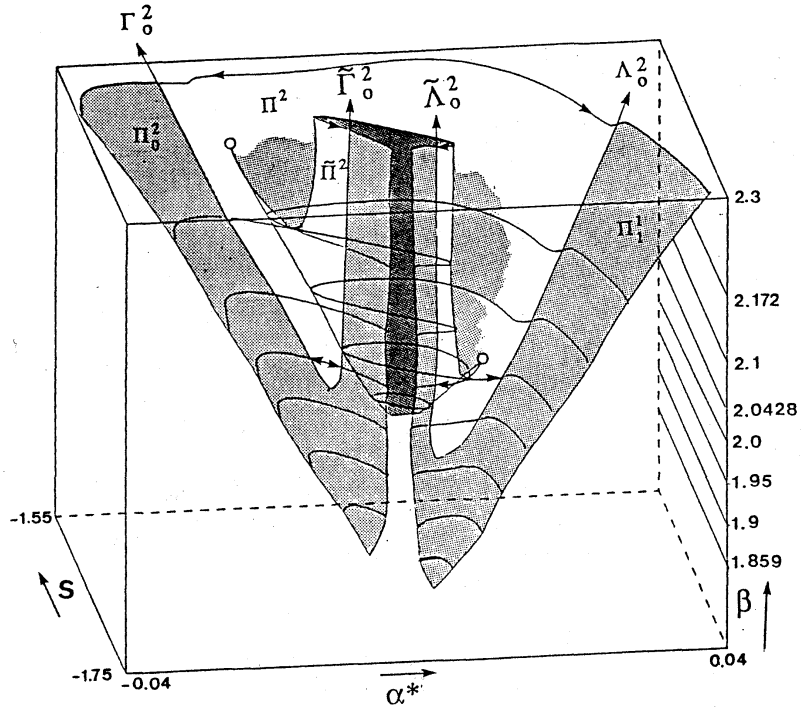

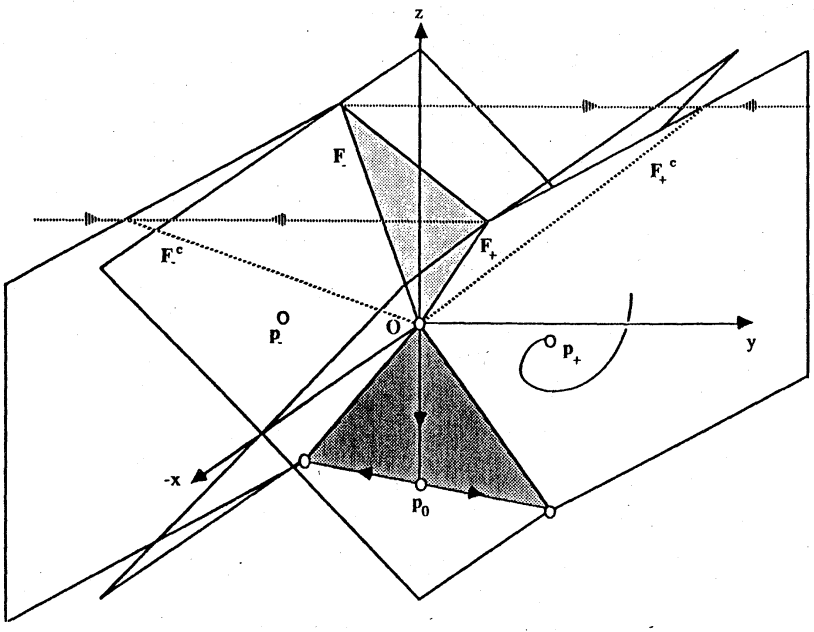

Figure 12

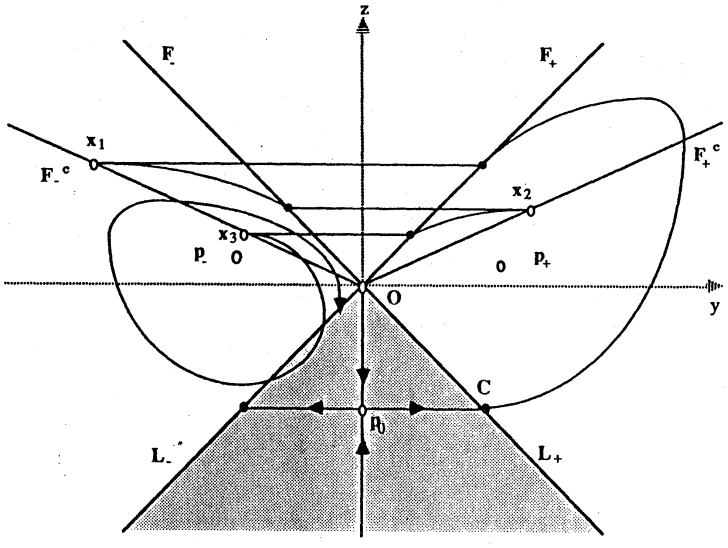

Figure 13

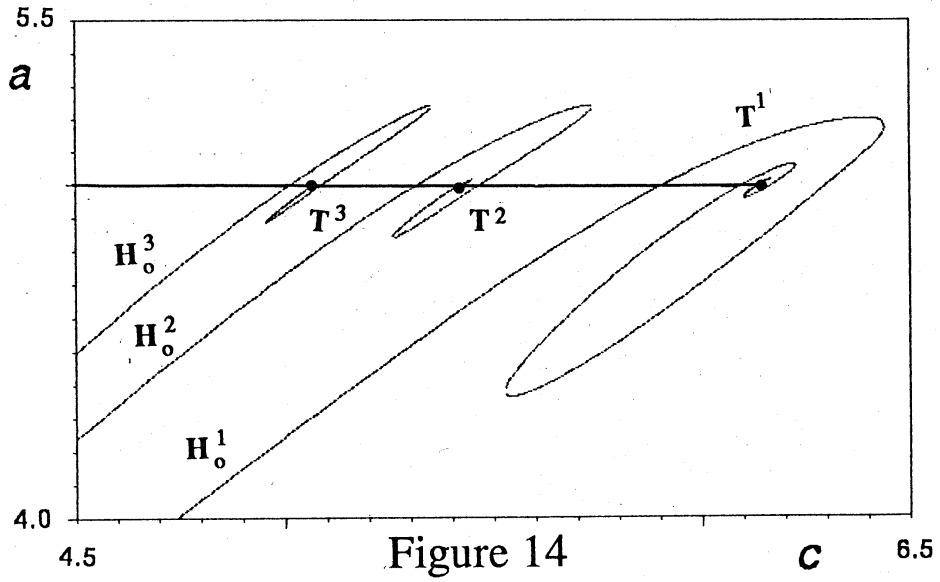

Figure 14

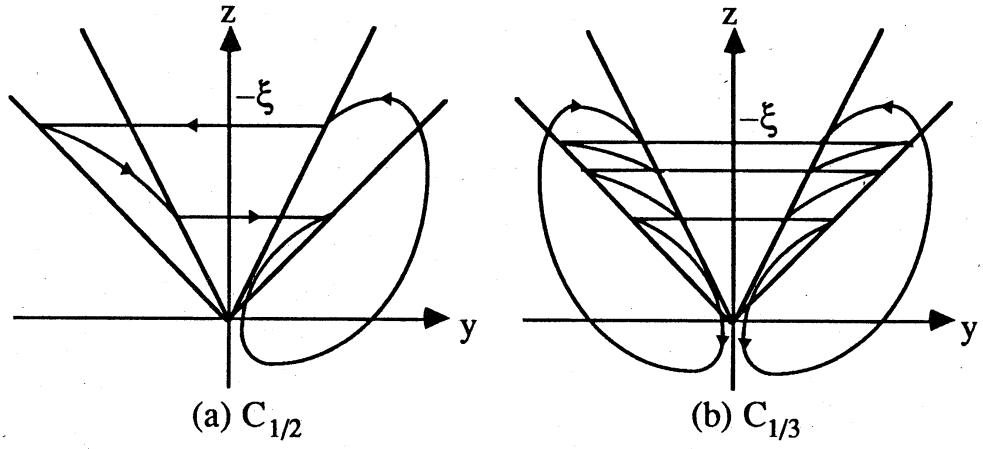

(a) $C_{1/2}$ (b) $C_{1/3}$

Figure 15

Figure 16

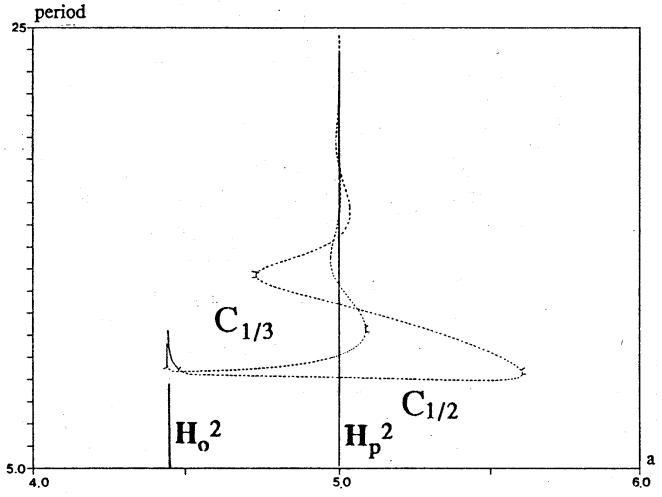

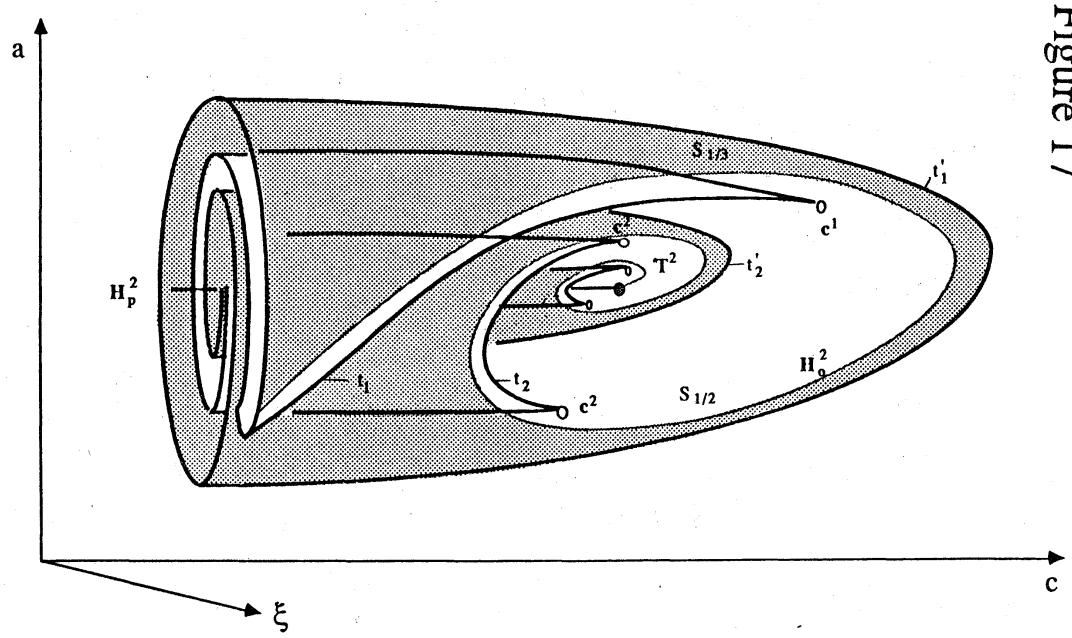

Figure 17

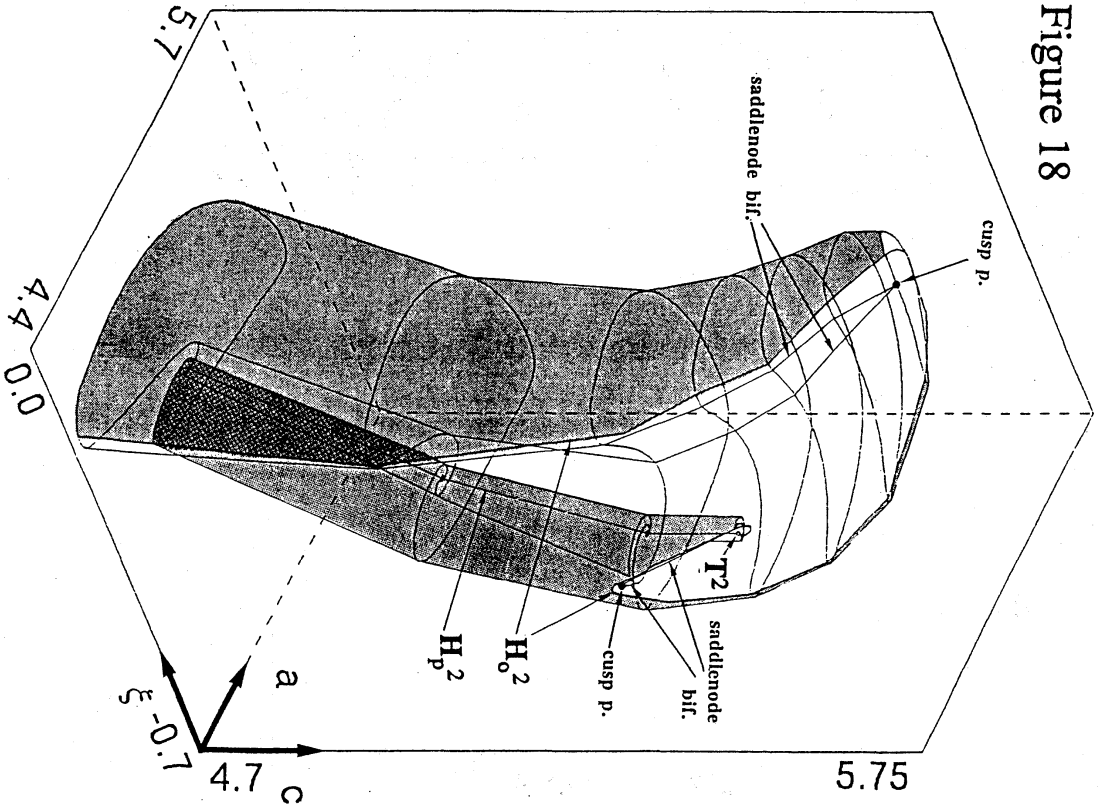

Figure 18

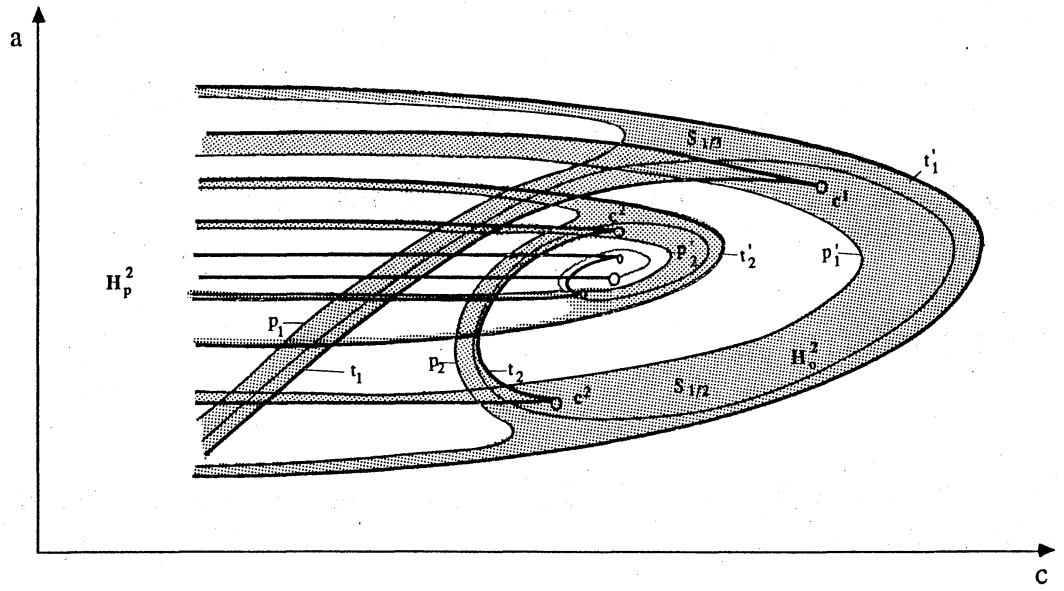

Figure 19